Supporting Information

Parameterized yields of semi-volatile products from isoprene oxidation under different NO_x levels: impacts of chemical aging and wall-loss of reactive gases

Li Xing, [†,‡,§] ***Manish Shrivastava,*** [*,‡] ***Tzung-May Fu,*** [*,†] ***Pontus Roldin,*** [‖] ***Yun Qian,*** [‡] ***Lu Xu,*** [⊥,#] ***Nga L. Ng,*** [⊥,▽] ***John Shilling,*** [‡] ***Alla Zelenyuk,*** [‡] ***and Christopher D. Cappa*** [○]

[†] Department of Atmospheric and Oceanic Sciences and Laboratory for Climate and Ocean-Atmosphere Studies, School of Physics, Peking University, Beijing, 100871, China

[‡] Pacific Northwest National Laboratory, Richland, Washington, 99352, USA

[§] Key Lab of Aerosol Chemistry & Physics, State Key Laboratory of Loess and Quaternary Geology, Institute of Earth Environment, Chinese Academy of Sciences, Xi'an, 710061, China

[‖] Division of Nuclear Physics, Lund University, P.O. Box 118, 221 00 Lund, Sweden

[⊥] School of Chemical and Biomolecular Engineering, Georgia Institute of Technology, Atlanta, Georgia 30332, USA

[#] Division of Geological and Planetary Sciences, California Institute of Technology, Pasadena, California 91125, USA

[▽] School of Earth and Atmospheric Sciences, Georgia Institute of Technology, Atlanta, Georgia 30332, USA

[○] Department of Civil and Environmental Engineering, University of California, Davis, California, 95616, USA

* Corresponding authors: M. Shrivastava (ManishKumar.Shrivastava@pnnl.gov) and T.-M. Fu (tmfu@pku.edu.cn)

S1 Non-continuum correction factor for the mass growth rate of particles

For the diffusive growth of a particle of diameter D_p, the Knudsen number Kn was calculated as $Kn=\lambda_{j,i}/D_p$, where $\lambda_{j,i}$ was the mean free path of the generation-j organic gas in the i^{th} volatility bin ($G_{j,i}$):

$$\lambda_{j,i} = \frac{3D_{gas}}{\sqrt{8RT/\pi M_{j,i}}} \quad \text{Eq (S1)}$$

D_{gas} was the gas diffusion coefficient of the organic gases (0.05 $cm^2\ s^{-1}$).[1] R was the universal gas constant (8.314 J $mol^{-1}\ K^{-1}$). T was the temperature in units of K. $M_{j,i}$ was the molar mass of organic gas $G_{j,i}$ (set to a constant of 250 g mol^{-1}). The correction factor for non-continuum conditions was

$$f(Kn,a) = \frac{1}{1+2Kn/a} \quad \text{Eq (S2)}$$

S2 Representation of the loss of particles to chamber walls in the box model

We implemented the particle wall-loss module from the Aerosol Dynamics, gas- and particle-phase chemistry model for laboratory CHAMber studies (ADCHAM)[2] into our box model to simulate the loss of particles to chamber walls. In the module, the loss of particles to chamber walls was analogous to particle migration in an effective electrical field and could be represented by a first-order deposition rate.[2] The particles suspended in the chamber were assigned zero, one, two, or three elemental charges assuming a Boltzmann charge distribution in

each size bin. The total deposition rate in each size bin was the number-weighted-mean of the deposition rates for the zero, one, two, and three charged particles.

For zero-charge particles, the first-order deposition rate to the chamber walls was calculated following Lai and Nazaroff[3], assuming that the turbulence in the chamber was homogeneous and isotropic. The deposition velocities for the vertical surfaces (k_{dv}), the upward horizontal surface (k_{du}), and the downward horizontal surface (k_{dd}) were calculated by Eq (S3-S5):

$$k_{dv} = \frac{\mu^*}{I} \qquad \text{Eq (S3)}$$

$$k_{du} = \frac{v_s}{1-\exp(-\frac{v_s I}{\mu^*})} \qquad \text{Eq (S4)}$$

$$k_{dd} = \frac{v_s}{\exp(\frac{v_s I}{\mu^*})-1} \qquad \text{Eq (S5)}$$

where μ* was the friction velocity, which was unknown for PNNL chamber and needed to be fitted. I was a parameterized integral related to the flux of particles across the boundary layer and calculated by the equations in Table 2 from Lai and Nazaroff[3] (not listed in detail here). v_s was the terminal setting velocity of a particle with a diameter of D_p:

$$v_s = \frac{1}{18}\frac{D_p^2 \rho g C_c}{\mu} \qquad \text{Eq (S6)}$$

μ was the dynamic viscosity of air in the chamber (1.8×10^{-5} kg m^{-1} s^{-1}). C_c was the Cunningham slip correction factor:

$$C_c = 1 + \frac{2\lambda_i}{D_p}[1.257 + 0.4\exp(-\frac{1.1 D_p}{2\lambda_i})] \qquad \text{Eq (S7)}$$

The deposition rate for non-charged particles, $k_{\text{non-charge}}$ (s^{-1}) was calculated by Eq (S8):

$$k_{\text{non-charge}} = \frac{k_{dv}A_v + k_{du}A_u + k_{dd}A_d}{V} \qquad \text{Eq (S8)}$$

where A_v, A_u, and A_d were the surface areas of the vertical surfaces, the upward-facing surface, and the downward-facing surface, respectively. V was the volume of the chamber.

For the charged particles, the first-order deposition rate, k_{charge} (s^{-1}), for particles of diameter D_p was calculated by Eq (S9):

$$k_{\text{charge}} = \frac{A}{V}\frac{neC_cE}{3\pi\mu D_p} \qquad \text{Eq (S9)}$$

where A was the chamber surface area, V was the chamber volume, n was the number of elemental charges of the particle, e was the elementary charge, E was the mean electrical field strength.

The effective electrical field strength E in Eq (S9) and the friction velocity μ^* in Eq. (S3-S5) were two unknown and tunable parameters in our box model, which could be fitted using experimental data. Xu et al.[4] injected ammonium sulfate particles into the PNNL chamber and used the SMPS to monitor the temporal evolutions of the particle number concentration and size distribution. We varied the values of E and μ^* in our box model (with no gas- and aerosol-phase chemistry) to find the best fit to the observed total number concentration and size distribution (Figure S1). The resulting optimized values for E and μ^* in the PNNL chamber were 10 V cm^{-1} and 0.14 m s^{-1}, respectively.

To further evaluate our particle wall-loss calculation, we also simulated the SOA concentrations using our best-fit chemical scenarios and product yields with the particle wall-loss calculations turned off. We compared the results to the particle wall-loss corrected SOA mass concentration measurements from Xu et al.[4], as shown in Figure S2. We found that our box

model, in addition to being able to fit the raw measured time series of SOA mass (as shown in the main text), was also able to reproduce the measured wall-loss-corrected time series of SOA mass, especially in the latter half of the experiment. This indicates that our particle wall-loss calculation is consistent with the wall-loss corrections applied to the SOA measurements in Xu et al.[4].

S3 Representation of the irreversible loss of semi-volatile gases to chamber walls in the box model

In our box model, we included the irreversible deposition of semi-volatile organic gases onto chamber walls. The rationale for the irreversibility assumption was threefold. Firstly, chamber measurements by Zhang et al.[5] and Ye et al.[6] showed that the wall-loss of several semi-volatile gases (including several semi-volatile products from isoprene oxidation) was irreversible/quasi-irreversible in Teflon chambers with surface-to-volume ratios that were similar to the PNNL chamber at around 25^{o}C. Secondly, Zhang et al.[5] showed that the mass accommodation coefficient (a_w) of semi-volatile gases increases with decreasing volatility. Thirdly, Zhang et al.[5] used their parameterization for a_w to simulate the concentrations of semi-volatile gases in the Caltech chamber. They found that sensitivity simulations assuming either reversible or irreversible wall-loss both matched the measured semi-volatile gas concentrations up to approximately 18 hours into the experiment.

The quasi-irreversible deposition rate for the semi-volatile gases in the i^{th} volatility bin to chamber walls was calculated as:[5]

$$\frac{dC_i}{dt} = -\frac{A}{V}\left(\frac{a_{w,i}v_i/4}{\pi a_{w,i}v_i/8\sqrt{D_{\text{gas}}K_e}+1}\right)\cdot C_i \qquad \text{Eq (S10)}$$

where $a_{w,i}$ was the mass accommodation coefficient on the wall for the semi-volatile gases in the i^{th} volatility bin, v_i was the mean thermal speed, and K_e was the eddy diffusion coefficient.

$$v_i = \sqrt{\frac{3RT}{M_i}} \qquad \text{Eq (S11)}$$

We first estimated the value of K_e for the PNNL chamber. We fitted the observed size-dependent deposition rates of ammonium sulfate particles ($k_{w,\text{particles}}$) from Xu et al.[4] by tuning a parameterization for particle deposition rate from Zhang et al.[7]:

$$k_{w,\text{particles}} = \frac{A}{V}\left[\frac{8\sqrt{K_eD}}{\pi} + v_s\cdot\coth\left(\frac{x}{2}\right)\right] \qquad \text{Eq (S12)}$$

where D was the particle diffusion coefficient and v_s was the particle terminal settling velocity (Eq S6). D and x were calculated as in Eq (S13) to Eq (S14):[8]

$$D = \frac{kTC_{\text{c}}}{3\pi\mu D_{\text{p}}} \qquad \text{Eq (S13)}$$

$$x = \frac{\pi v}{2\sqrt{K_eD}} \qquad \text{Eq (S14)}$$

where g was the earth gravitational constant and k was the Boltzmann constant. We found that a best-fit value of K_e = 0.006 s^{-1} for the PNNL chamber resulted in a good agreement between the observed and parameterized size-dependent particle deposition rates, as shown in Figure S3.

Zhang et al.[5] showed that $\log_{10}a_{w,i}$ decreased linearly with $\log_{10}C^*_i$, as described in Eq (S14):

$$log_{10}a_{w,i} = -0.1919\times log_{10}C_i^* - b \qquad \text{Eq (S15)}$$

where b = 6.32 for the Caltech Teflon chamber. To find the appropriate value of b for the PNNL chamber, we simultaneously varied the value of b in Eq (S15) and the generation-one product yields α_i in our box model using a "Non-aging" chemical scenario in the HO_2-dominant experiment. We then looked for the combination of b and α_i that led to the best fit of the measured time series of SOA mass, as described in the fitting procedure in the main text. In the end, we selected the value b =6.04 as the best-fit for the PNNL chamber. The corresponding set of values of $a_{w,i}$ were 1.43×10^{-6}, 9.12×10^{-7}, 5.89×10^{-7}, 3.8×10^{-7} for the semi-volatile gases with saturation vapor concentrations C^* = 0.1, 1, 10, 100 μg m^{-3}, respectively.

S4 Comparison of simulated and measured particle size distribution

Figure S4 compared the temporal evolution of the particle size distributions simulated by our box model (using the best-fit chemical scenarios and product yields) against the measurements by Xu et al.[4] We found that our box model was able to reproduce the temporal evolution of the measured SOA size distributions, indicating that the particle wall-loss and aerosol microphysical processes were well represented in our box model.

For each of the three experiments at different levels of NO_x, the simulated particle size distributions assuming the two best-fit chemical scenarios were very similar. As a result, it was not possible to determine which one of the two best-fit chemical scenarios was more appropriate based on the particle size distribution evolution. This is not surprising, as we used the observed initial particle size distribution at t_0 as *de facto* seeds to initialize our model and subsequently fitted the generation-one product yields in our box model to match the measured SOA mass

evolution. As such, the particle number and total particle mass in our fitted simulations were both strongly constrained by the observations.

S5 Validation of best-fit chemical scenarios and product yields against additional chamber measurements

To further validate our parameterized product yields, we used our best-fit chemical scenarios and product yields to simulate the SOA concentrations in the five additional chamber experiments in Xu et al.[4], as shown in Figure S5. Note that the experiments in Xu et al.[4] were conducted in different Teflon bags: experiments 1, 4, and 5 were conducted in Bag A, while experiments 2, 3, 6, 7, and 8 were conducted in Bag B. The particle wall-loss rate for Bag A was three times larger than that of Bag B. To make the SOA mass concentrations across different experiment comparable, the SOA mass measurement shown in Figure S5 were corrected for particle wall-loss, and the simulations were conducted with the particle wall-loss calculations turned off. The initial NO_x concentrations for experiment 1 and 3 was below 1 ppb; the initial NO_x-to-isoprene ratios for experiment 4, 5, and 7 were 0.7, 1.26, and 4.42, respectively. We characterized experiments 1 and 3 as "HO_2-dominant" experiments, experiments 4 and 5 as "intermediate-NO_x mixed" experiments, and experiment 7 as a "high-NO_x mixed" experiment. We simulated each of these five experiments using the recommended chemical scenarios and product yields obtained for the corresponding NO_x conditions.

Figure S5 shows the comparison between measured and simulated time series of SOA mass concentrations. For the HO_2-dominant experiments (experiments 1 and 3), the FragH_OligS_P scneario was able to better reproduce the measured SOA. For the intermediate-NO_x mixed experiments (experiments 4 and 5), the FragL_OligS scenario performed better than the

FragL_OligF scenario. The FragL_OligF reproduced the peak SOA mass concentration but overestimated the SOA mass at longer times. For the high-NO_x mixed experiment (experiment 7), the FragM_OligF scenario simulated the measured SOA better than the the FragM_OligS scenario did. Overall, the correlation coefficients between the measured and simulated SOA mass time series all exceeded 0.8., except for the simulations with the FragL_OligF scenario in experiments 4 and 5. This indicated that the best-fit chemical scenarios and product yields obtained from fitting experiments 2, 6, and 8 in Xu et al.[4] was generally applicable to other experiments.

S6 Impacts of different gas-phase chemical aging rates and aerosol oligomerization rates on the parameterized yields of semi-volatile products

In our parameterization presented in the main text, we assumed that the lumped generation-one semi-volatile gas products were oxidized by OH to form lumped higher-generation products at a fixed rate constant $k_2 = 2\times10^{-11}$ cm^3 $molecule^{-1}$ s^{-1}. In reality, the value of k_2 is dependent on the reactivity of the lumped higher-generation semi-volatile products. Chamber experiments have indicated that, under high-NO_x conditions, the oxidation of isoprene by OH produces MACR as the main first-generation product, which further reacts with OH and NO_2 to produce MPAN.[4] Under low-NOx conditions, isoprene + OH produces ISOPOOH as the main first-generation product, which goes on to react with OH to produce IEPOX as a major product.[4] From Xu et al.[4], the reaction rates of MACR and ISOPOOH with OH were 2.9×10^{-11} and 7×10^{-11} cm^3 $molecule^{-1}$ s^{-1}, respectively. The reaction rates of MPAN and IEPOX with OH were 2.9×10^{-11} and 1.5×10^{-11} cm^3 $molecule^{-1}$ s^{-1}, respectively. We thus conducted additional fittings

for the HO_2-dominant experiment using the best-fit FragH_OligS_P scenario, while varying the value of k_2, to evaluate the impacts of the assumed k_2 value on the resulting parameterized semi-volatile product yields (Table S2). Figure S6 compares our best-fit simulated SOA mass concentrations using different k_2 values (1.5×10^{-11}, 2.0×10^{-11}, 7.0×10^{-11} cm^3 $molecule^{-1}$ s^{-1}) against the measurements. We found that our box model assuming all three k_2 values were able to fit the measured time series SOA well (correlation coefficients were 0.93, 0.94, and 0.95, respectively). Assuming larger values of k_2 (faster aging) in the model led to larger yields of the lower-volatility products (Table S2), which compensated the faster fragmentation of low-volatility products under the FragH_OligS_P scenario.

Similarly, we investigated the impacts on the parameterized semi-volatile product yields due to different aerosol oligomerization rates, which at present are not well constrained. We fitted the intermediate-NO_x mixed experiment assuming the best-fit FragL_Olig chemical scenario, except that the aerosol oligomerization time scales ($\tau_{olig} = 1/ k_{olig}$) were varied between 20 hours, 10 hours, 1 hour, and 10 minutes, respectively. The best-fit simulated time series of SOA mass are compared to the measurements in Figure S7, and the associated optimized product yields are shown in Table S3. We found that the different oligomerization rates could all fit the SOA mass ($r > 0.93$) reasonably well, although the faster oligomerization rates (τ_{olig} = 1 hour or 10 minutes) better captured the measured slow decay of SOA mass during the latter half of the experiments. We found that the assumption of faster oligomerization led to larger yields of the lower-volatility (C^* = 0.1 and 1 $\mu g\ m^{-3}$) products, likely to suppress SOA formation in the early stages of the experiment by allowing more wall-losses of the semi-volatile gases.

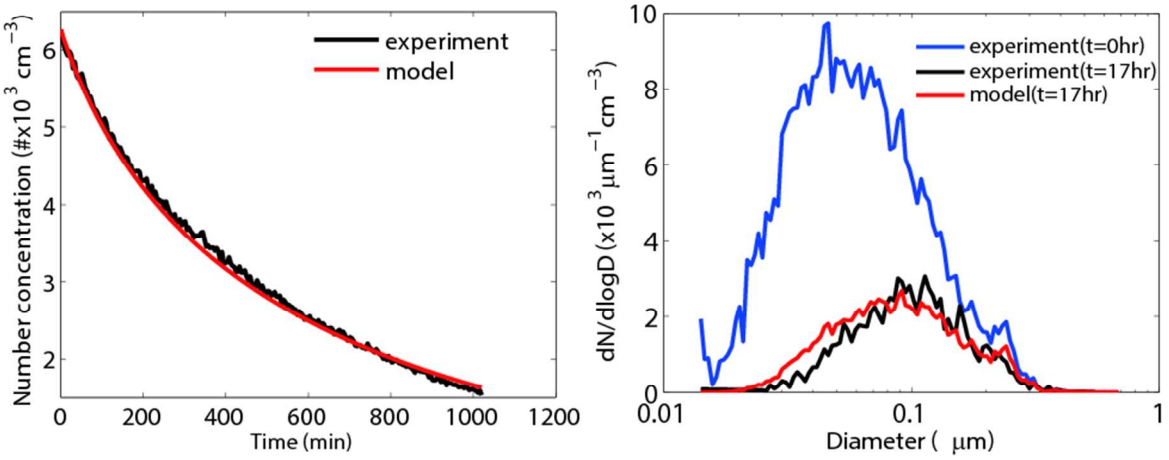

208

209 **Figure S1.** (a) Time series of the total number concentration of ammonium sulfate particles in
210 the PNNL chamber as measured by Xu et al.[4] (black) and as simulated by our box model (red).
211 (b) The size distributions of the ammonium sulfate particles in the PNNL chambers measured at t
212 = 0 hr (blue) and at t = 17 hr (black), as well as the size distribution simulated by our box model
213 at t = 17 hr (red). The temporal evolution of the particle numbers and size distribution in the box
214 model were mainly due to the loss of particles to chamber walls, which were simulated here
215 using the optimized values of E = 10 V cm^{-1} and μ^* 0.14 m s^{-1}, respectively.
216 Coagulation/coalescence processes were also accounted for in our box model but had lesser
217 impacts on the temporal evolution of the particle size distribution.

218

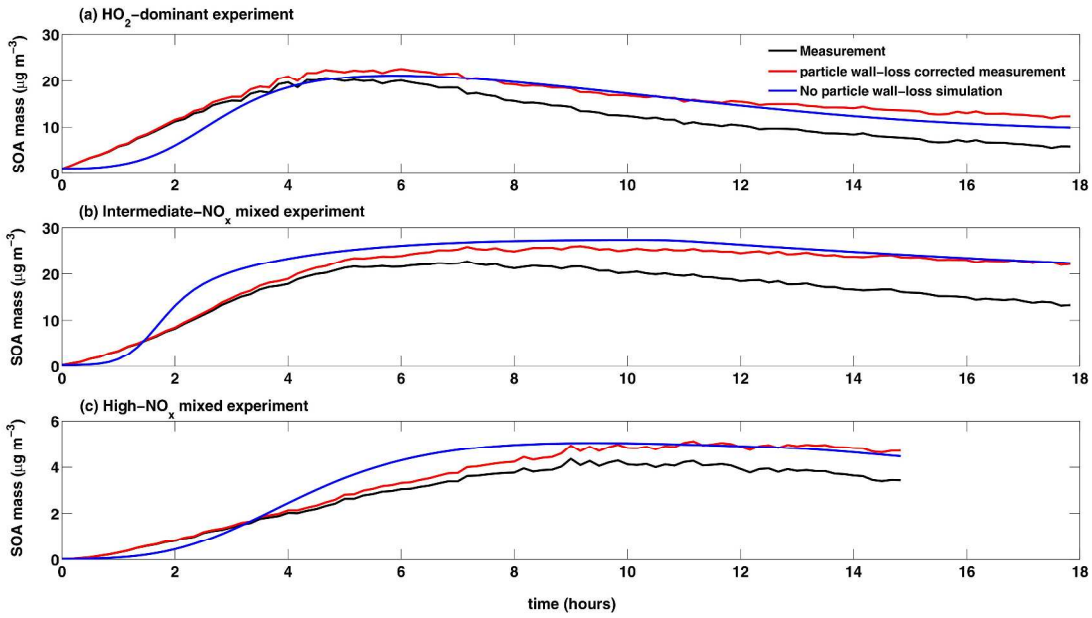

Figure S2. Comparison between the particle wall-loss corrected SOA mass measurement and the model simulated SOA mass concentrations with the particle wall-loss turned off for (a) the HO_2-dominant experiment, (b) the intermediate-NO_x mixed experiment, and (c) the High-NO_x mixed experiment. Black lines indicate the measurements without wall-loss correction, and red lines indicate the particle wall-loss corrected measurement. Blue lines denote the model simulation using the best-fit chemical scenarios and product yields with the particle wall-loss turned off.

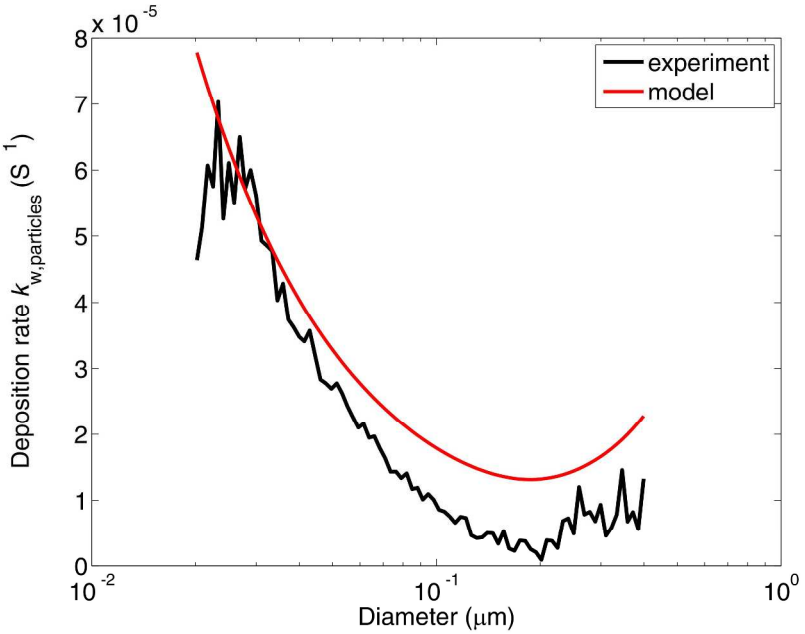

228

229 **Figure S3.** The observed deposition rates of ammonium sulfate particles (black) were used to

230 find the optimized value for the eddy diffusion coefficient (K_e) for the PNNL chamber. The

231 parameterized particle deposition rates using K_e = 0.006 (red) led to a good agreement with the

232 observation.

233

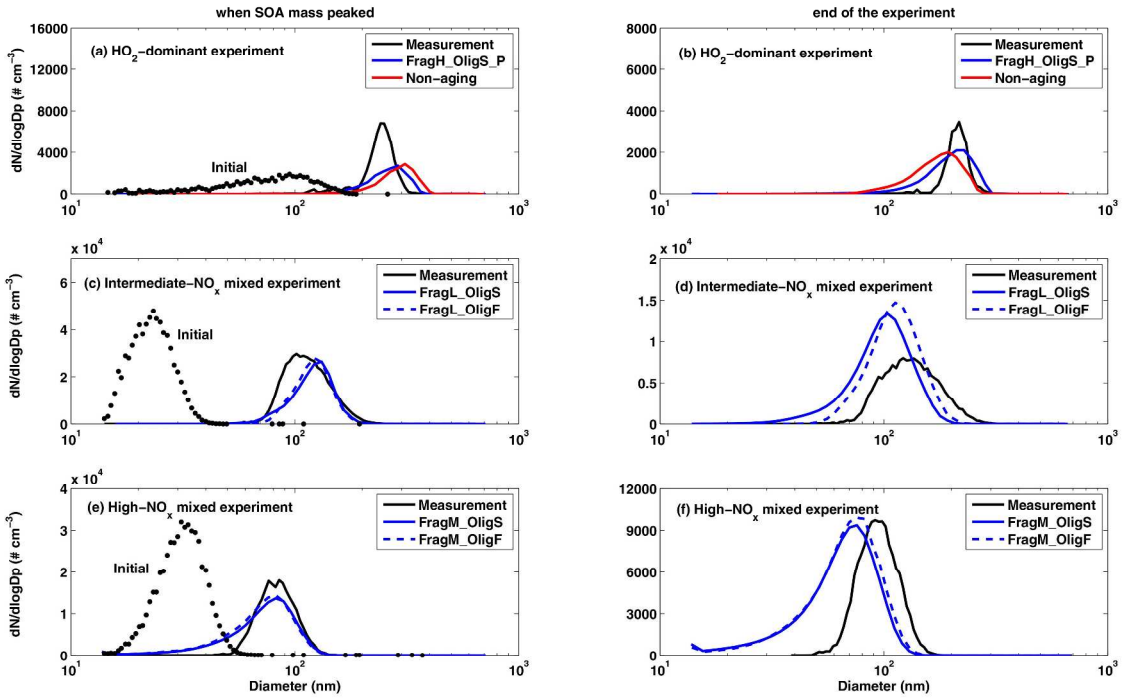

Figure S4. The comparison between observed and simulated size distribution for (a, b) HO_2-dominant experiment, (c, d) Intermediate-NO_x mixed experiment, and (e, f) High-NO_x mixed experiment. The black dots in the left panels showed the initial measured size distributions at t = t_0 (t_0 = 0.75 hours, 1 hour, and 3 hours for experiments 2, 6, and 8 in Xu et al.[4], respectively. See the main text for details). The left three panels showed the size distributions at the time when the SOA mass peaked, and the right three panels showed the size distributions at the end of the experiments.

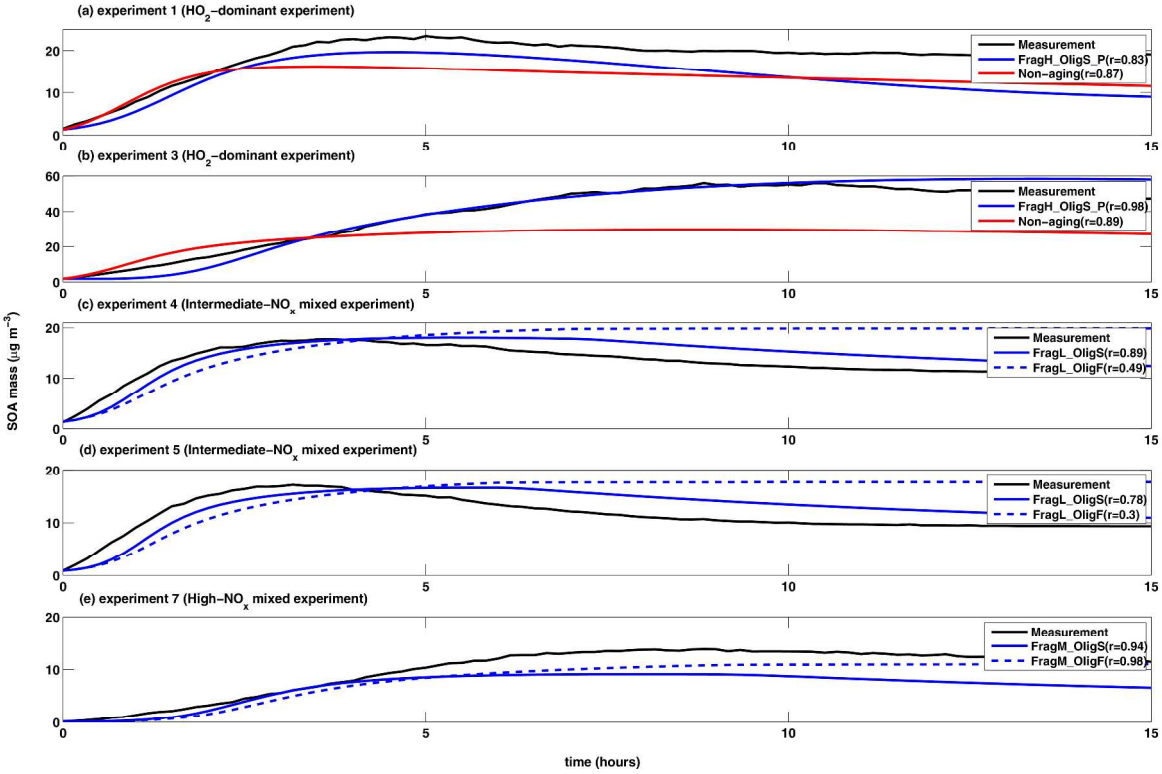

Figure S5. Comparison between the measured (black) and simulated (red and blue) SOA mass concentrations for (a) experiment 1, (b) experiment 3, (c) experiment 4, (d) experiment 5, and (e) experiment 7 in Xu et al.[4] The measured time series of SOA mass was corrected for particle wall-loss by Xu et al.[4] The simulations were conducted with the particle wall-loss calculations turned off.

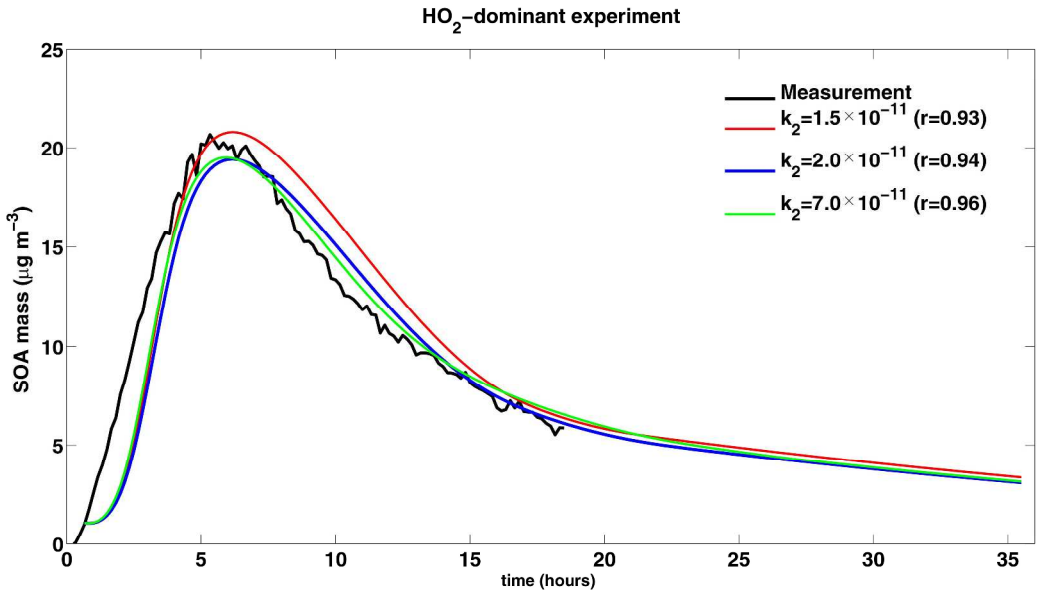

Figure S6. Observed and simulated time series of SOA mass for the HO_2-dominant experiment and assuming the FragH_OligS_P chemical scenario, given different assumed values of k_2. The model simulations shown here are the best-fit time series with optimized semi-volatile product yields (Table S2).

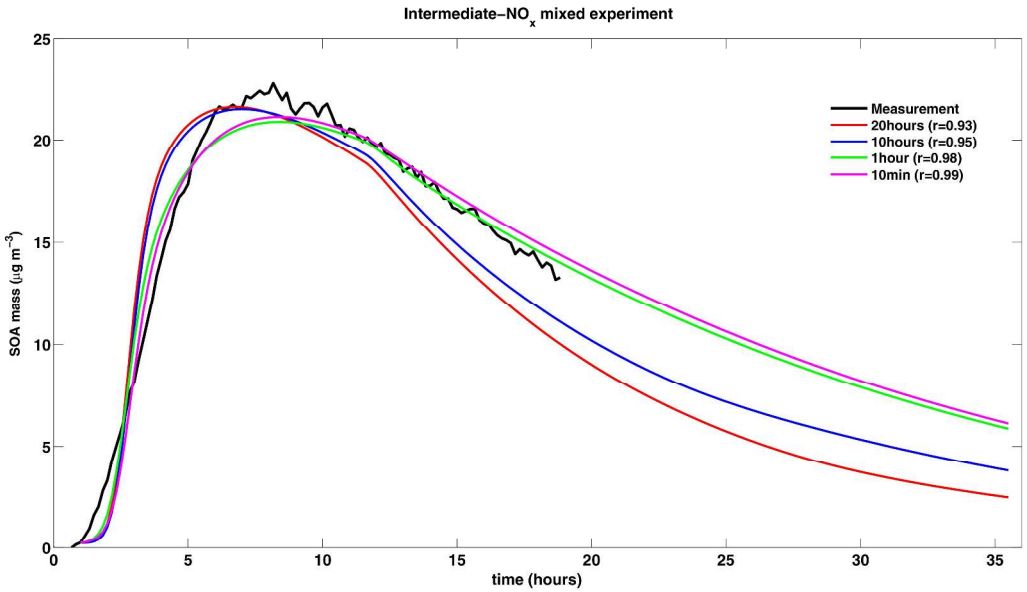

Figure S7. Observed and simulated time series of SOA mass for the intermediate-NO_x mixed experiment and assuming the FragL_Olig chemical scenario, given different values of τ_{olig}. The model simulations shown here are the best-fit time series with optimized semi-volatile product yields (Table S3).

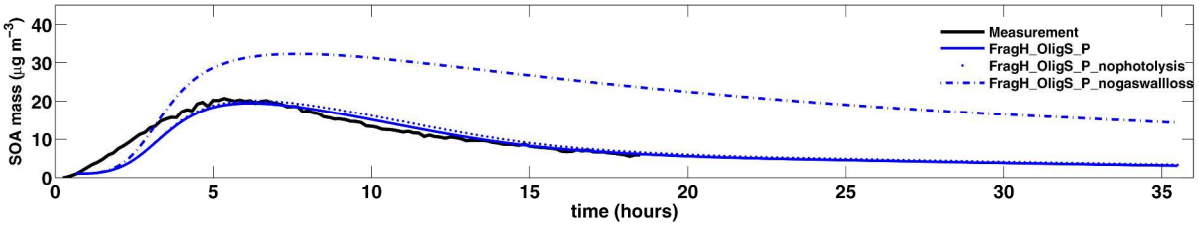

Figure S8. Observed (black) and simulated (blue) time series of SOA mass for the HO_2-dominant experiment. Solid blue line represents the FragH_OligS_P scenario. Dotted blue line represents the FragH_OligS_P scenario with the SOA photolysis turned off. Dashed blue line represents the FragH_OligS_P scenario with the gas wall-loss turned off.

Table S1 Gas- and aerosol-phase chemical reactions in the box model

Gas-phase chemical reactions	
$\text{Isoprene} + \text{OH} \xrightarrow{k_1} \alpha_i \cdot \text{G}_{1,i}$, for i = 1,2,3,4	R (S1)
$\text{G}_{j,1} + \text{OH} \xrightarrow{k_2} \text{BR}_{\text{frag}} \cdot \text{G}_{2,4} + 0.1 \cdot \text{G}_v + \left(1 - 0.1 - \text{BR}_{\text{frag}}\right) \cdot \text{G}_{2,1}$, for j = 1,2	R (S2a)
$\text{G}_{j,i} + \text{OH} \xrightarrow{k_2} \text{BR}_{\text{frag}} \cdot \text{G}_{2,4} + \text{BR}_{\text{func}} \cdot 1.15 \cdot \text{G}_{2,i-1} + 0.1 \cdot \text{G}_v$, for i = 2,3,4; j = 1,2	R (S2b)
Gas/aerosol diffusive mass growth/evaporation	
$\text{G}_{j,i} \overset{k_{\text{diff}}}{\longleftrightarrow} \text{SOA}_i$, for i = 1,2,3,4; j = 1,2	R (S3)
Aerosol-phase reactions	
$\text{SOA}_i \xrightarrow{k_{\text{olig}}} \text{NVSOA}$, for i = 1,2,3,4	R (S4)
$\text{SOA}_i \xrightarrow{J} \text{G}_v$, for i = 1,2,3,4	R (S5a)
$\text{NVSOA} \xrightarrow{J} \text{G}_v$	R (S5b)

Table S2 The impacts of gas-phase chemical aging rates on optimized product yields

Gas-phase aging rate k_2 [a]	C^* (μg m^{-3})			
	0.1	1	10	100
$k_2 = 1.5 \times 10^{-11}$ cm^3 molecule^{-1} s^{-1}	3.68×10^{-5}	3.68×10^{-5}	2.82×10^{-1}	7.40×10^{-2}
$k_2 = 2.0 \times 10^{-11}$ cm^3 molecule^{-1} s^{-1}	3.68×10^{-5}	5.52×10^{-4}	2.82×10^{-1}	6.44×10^{-2}
$k_2 = 7.0 \times 10^{-11}$ cm^3 molecule^{-1} s^{-1}	3.68×10^{-5}	9.20×10^{-3}	3.50×10^{-1}	1.80×10^{-3}

a All fittings were based on the FragH_OligS_P chemical scenario for the HO_2-dominant experiment, except that the gas-phase aging rate for semi-volatile products (k_2) was varied as specified in the Table.

Table S3 The impacts of aerosol oligomerization rates on optimized product yields (intermediate-NO_x mixed experiment)

Oligomerization time scales [a]	C^* (μg m^{-3})			
	0.1	1	10	100
τ_{olig} = 20 hours	3.68×10^{-5}	3.68×10^{-5}	1.80×10^{-3}	2.50×10^{-1}
τ_{olig} = 10 hours	3.68×10^{-5}	3.68×10^{-5}	2.61×10^{-4}	2.50×10^{-1}
τ_{olig} = 1 hour	1.80×10^{-3}	5.52×10^{-4}	4.42×10^{-3}	2.18×10^{-1}
τ_{olig} = 10 minutes	1.80×10^{-3}	2.61×10^{-4}	1.80×10^{-3}	2.18×10^{-1}

a All fittings were based on the FragL_OligS chemical scenario for the intermediate-NO_x mixed experiment, except that the aerosol oligomerization time scale (τ_{olig}) was varied as specified in the table. The first-order aerosol oligomerization rate $k_{olig} = 1/\ \tau_{olig}$.

References

(1) Zaveri, R. A.; Easter, R. C.; Shilling, J. E.; Seinfeld, J. H. Modeling kinetic partitioning of secondary organic aerosol and size distribution dynamics: representing effects of volatility, phase state, and particle-phase reaction. *Atmos. Chem. Phys.* **2014**, 14, 5153-5181.

(2) Roldin, P.; Eriksson, A. C.; Nordin, E. Z.; Hermansson, E.; Mogensen, D.; Rusanen, A.; Boy, M.; Swietlicki, E.; Svenningsson, B.; Zelenyuk, A.; Pagels, L. Modelling non-equilibrium secondary organic aerosol formation and evaporation with the aerosol dynamics, gas- and particle-phase chemistry kinetic multilayer model ADCHAM. *Atmos. Chem. Phys.* **2014**, 14, 7953-7993.

(3) Lai, A.; Nazaroff, W. W. Modelling indoor particle deposition from turbulent flow onto smooth surfaces. *J. Aerosol Sci.* **2000**, 31, 463–476.

(4) Xu, L.; Kollman, M. S.; Chen, S.; Shilling, J. E.; Ng, N. L. Effects of NOx on the volatility of secondary organic aerosol from isoprene photooxidation. *Environ. Sci. Technol*. **2014**, 48, 2253-2262.

(5) Zhang, X.; Schwantes, R. H.; McVay, R. C.; Lignell, H.; Coggon, M. M.; Flagan, R. C.; Seinfeld, J. H. Vapor wall deposition in Teflon chambers. *Atmos. Chem. Phys.* **2015**, 15, 4197-4214.

(6) Ye, P.; Ding, X.; Hakala, J.; Hofbauer, V., Robinson, E. S; Donahue, N. M. Vapor wall loss of semi-volatile organic compounds in a Teflon chamber. *Aerosol Sci. Technol.* **2016,** 50, 822-834.

(7) Zhang, X.; Cappa, C. D.; Jathar, S. H.; McVay, R. C.; Ensberg, J. J.; Kleeman, M. J.; Seinfeld, J. H. Influence of vapor wall loss in laboratory chambers on yields of secondary organic aerosol. *Proc. Natl. Acad. Sci. U.S.A.* **2014**, 111, 5802–5807.

(8) Seinfeld, J. H.; Pandis, S. N. Atmospheric Chemistry and Physics: From Air Pollution to Climate Change (2nd ed.). John Wiley & Sons, Inc., Hoboken, NJ, 2006.